Supplementary Information:

Tunable Band Alignment with Unperturbed Carrier Mobility of On-Surface Synthesized Organic Semiconducting Wires

Andrea Basagni,[1] Guillaume Vasseur,[2,3] Carlo A. Pignedoli,[4] Manuel Vilas-Varela,[5] Diego Peña,[5] Louis Nicolas,[1,6] Lucia Vitali,[3,7] Jorge Lobo-Checa,[8,9] Dimas G. de Oteyza,[2,3,7,*] Francesco Sedona,[1,*] Maurizio Casarin,[1] J. Enrique Ortega,[2,3,10] Mauro Sambi.[1,11]

[1]Dipartimento di Scienze Chimiche Università Degli Studi di Padova, Padova, Italy,

[2]Donostia International Physics Center (DIPC), Paseo Manuel Lardizabal 4, E-20018 San Sebastián, Spain

[3]Centro de Física de Materiales (CSIC/UPV-EHU) -Materials Physics Center, Paseo Manuel Lardizabal 5, E-20018 San Sebastián, Spain

[4]NCCR MARVEL, Empa, Swiss Federal Laboratories for Materials Science and Technology, Dübendorf, Switzerland,

[5]Centro de Investigación en Química Biolóxica e Materiais Moleculares (CIQUS) and Departamento de Química Orgánica, Universidade de Santiago de Compostela, 15782, Spain

[6]École Normale Supérieure de Cachan, Cachan, France,

[7] Ikerbasque, Basque Foundation for Science, 48013 Bilbao, Spain

[8] Instituto de Ciencia de Materiales de Aragón (ICMA), CSIC-Universidad de Zaragoza, E-50009 Zaragoza, Spain.

[9] Departamento de Física de la Materia Condensada, Universidad de Zaragoza, E-50009 Zaragoza, Spain.

[10] Departamento de Fisica Aplicada I, Universidad del Pais Vasco, E-20018 San Sebastián, Spain

[11] Consorzio INSTM, Unità di Ricerca di Padova, Padova, Italy

*Corresponding authors
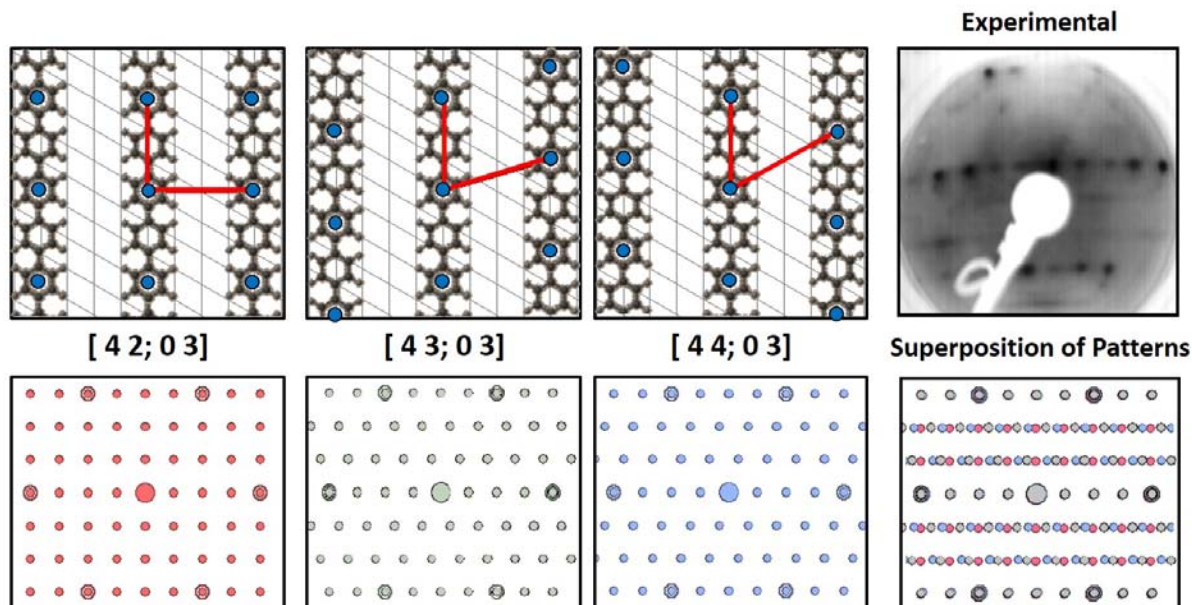d_g_oteyza@ehu.eus
francesco.sedona@unipd.it

Figure S1: PPP wires on the Au(887) substrate: direct and reciprocal space representations of the three

commensurate unit cells arising from different shifts between neighboring PPP chains along the $[1\bar{1}0]$ substrate direction. The experimental LEED pattern and the one obtained by superimposing the three simulated reciprocal lattices is shown on the right.
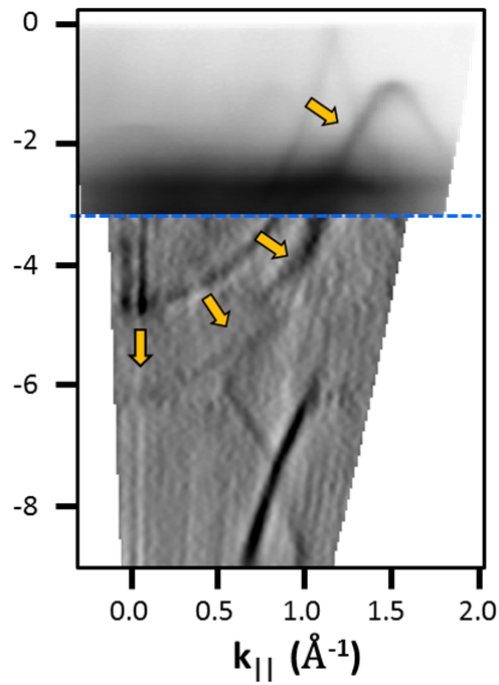

Figure S2: PPP wires on the Au(887) substrate: superposition of original ARPES (upper part) and second derivative ARPES (lower part). The derivative part highlights the dispersion of the band (yellow arrows) originating from the polymeric sheet, which disperses all the way from the VBM at E=-1.04 eV (k_x=1.49 Å^{-1}) down to E=-6.3 eV at Γ .
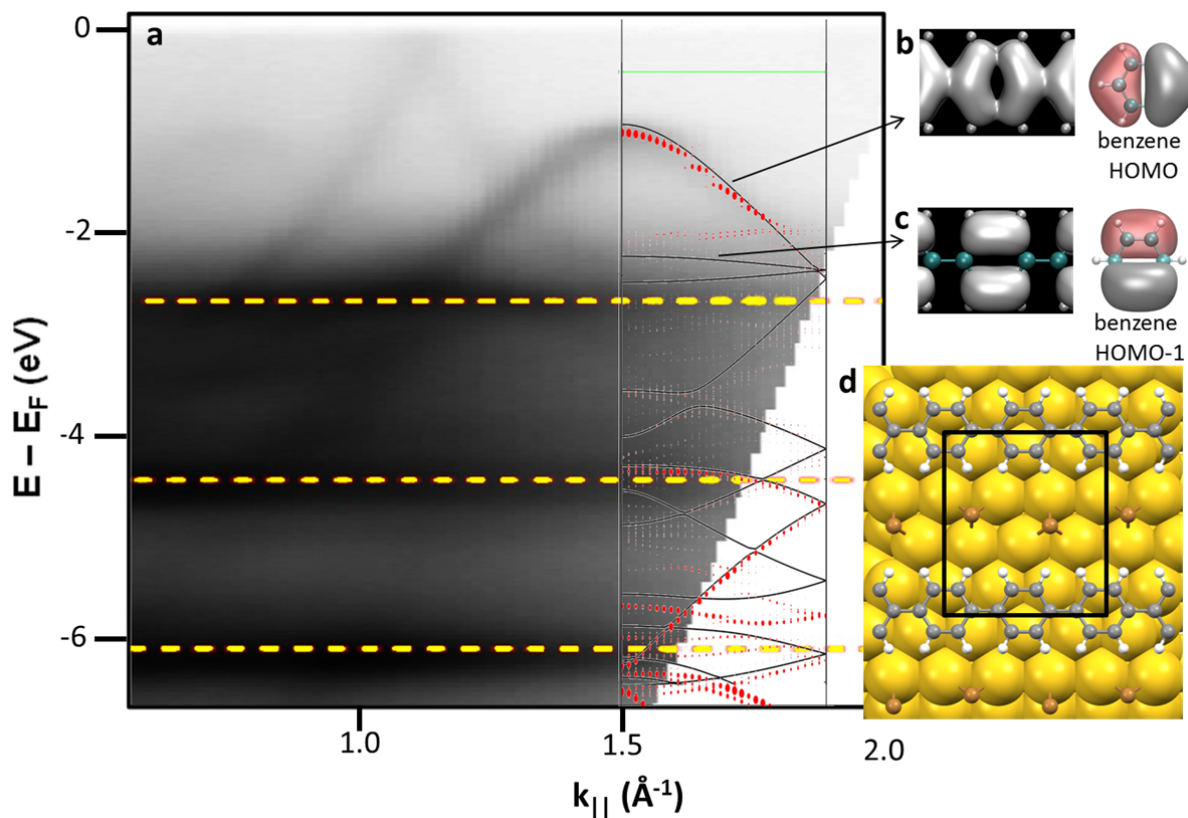
Figure S3: a) Overlap of experimental ARPES and DFT calculated band structure for PPP wires on Au(887). b) and c) PPP in gas phase: isosurface of the modulus of the Kohn-Sham (KS) orbital for the main dispersive band and the first quasi-flat band at $k_\parallel$=0.17 Å^{-1}, (left panels), rationalized as originating from benzene HOMO and HOMO-1 levels (right panels), respectively, associated to each of the phenyl rings along the chain. d) The model used for the DFT simulation: in-between the infinite PPP wires Br atoms are adsorbed on the substrate, in agreement with previous work on this system[1] (color code C gray, H white, Br orange, Au yellow). In the simulated band structure red circles are the carbon-projected bands of the reported model (carbon contribution is proportional to the diameter of the circles) and black lines are the bands of PPP wires in vacuum (i.e. without the substrate and Br atoms) constrained to the same geometry as on the surface. The energy of the calculated data has been rigidly shifted by -0.2 eV to fit the valence band maximum of the adsorbed PPP wires at $k_\parallel$=1.49 Å^{-1} to the experimental value.

Simulated data well reproduce the main features of experimental ARPES, such as the curvature of the main PPP dispersive valence band. It is interesting to note that at the energies of the three experimental non-dispersive bands (yellow dotted lines) the simulated data predict the appearance of quasi-flat bands.

Comparison of the shape and the energy of the simulated projected bands with and without the inclusion of the substrate (red circles and black lines, respectively) evidence a negligible effect of the gold surface on the top valence band curve.
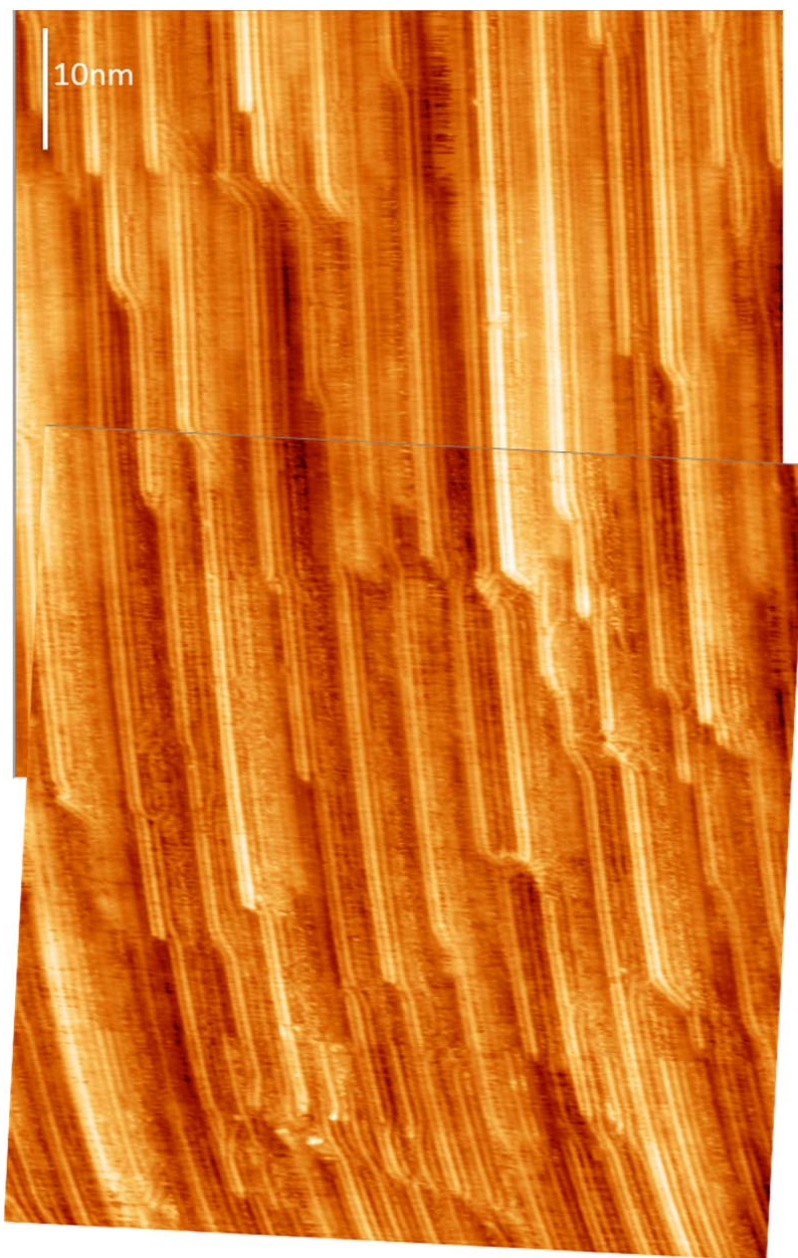
Figure S4: Overlapping STM images (V=0.60 V I=0.63 nA) revealing the length of the average wires to greatly exceed 8 nm, the value above which the polymer chain's electronic structure can be considered similar to that of infinitely long polymers.
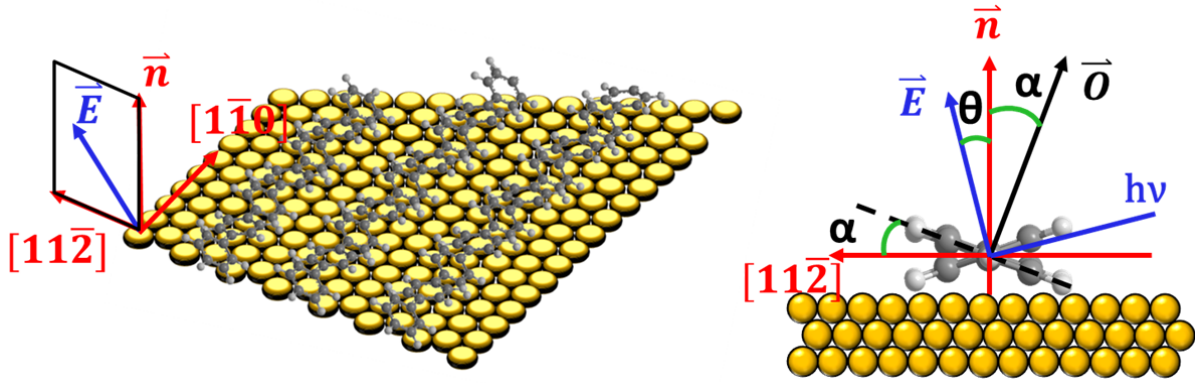
Figure S5: Graphical representation of the experimental geometry during the NEXAFS measurements. The X-rays strike the surface in the plane formed by the $[11\bar{2}]$ direction and the surface normal ($\vec{n}$). θ is the angle between the electric field $\vec{E}$ and $\vec{n}$; the angle defined by the axis of the π-like final-state orbital $\vec{O}$ and $\vec{n}$ is indicated with α.

The intensity of the transition can be derived from the Fermi golden rule:

$I \propto |\langle f|\mathbf{E} \cdot \mathbf{p}|i\rangle|^2$ In a simpler form: $I = A\left[\cos(\alpha \pm \theta)\right]^2$

Where **E** is the electric field vector, **p** the dipole operator, A the angle integrated cross section and $\alpha \pm \theta$ the possible values of angle between the electric field vector and the axis of the final-state orbital.

If one considers that adjacent phenyls are alternately rotated clockwise and counter-clockwise with respect to the polymer main axis due to the steric repulsion between hydrogen atoms facing each other from orto-positions to the inter-phenyl C-C bonds and due to the twofold symmetry of the vicinal surface, the NEXAFS dichroism is described by:

$$I = A\left(\cos(\alpha - \theta)\right)^2 + A\left(\cos(\alpha + \theta)\right)^2$$

This Stöhr-derived equation has been used to obtain the orientation of the phenyl rings with respect to the surface.[2]
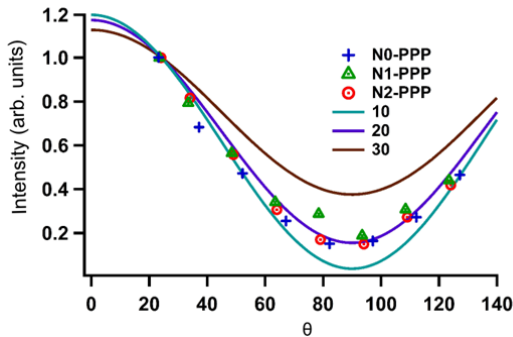

Figure S6: Angular dependence of the $\pi_1{}^*$ resonance intensity compared to the calculated behavior for different tilt angles of the phenyl rings on each of the studied polymer chains. The calculated curves have been normalized to the first experimental value at $\theta=30°$ for better comparison and reveal a similar tilt angle of 20° for all samples.
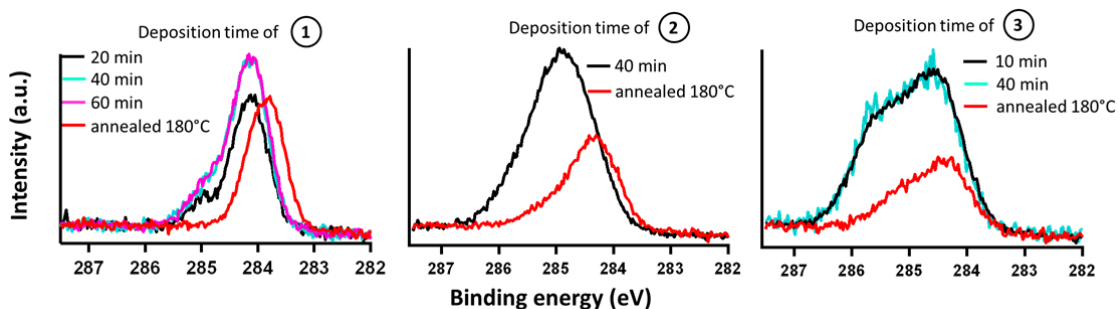
Figure S7: X-ray photoelectron spectroscopy data of the sample throughout the polymer preparation procedure: C 1s peak (hv=400 eV) as a function of the deposition time. Au(887) was held at RT while the molecular sources were at 105°C , 100°C and 90°C for precursors 1, 2 and 3 (see Figure 1), respectively. Sublimation has been protracted until the C 1s intensity saturated and further sublimation did not result in an increase of the signals. The heating treatment at 180°C caused desorption of the multilayer, leaving the samples fully covered with a single molecular monolayer of poly-para-phenylene wires adsorbed on the substrate.
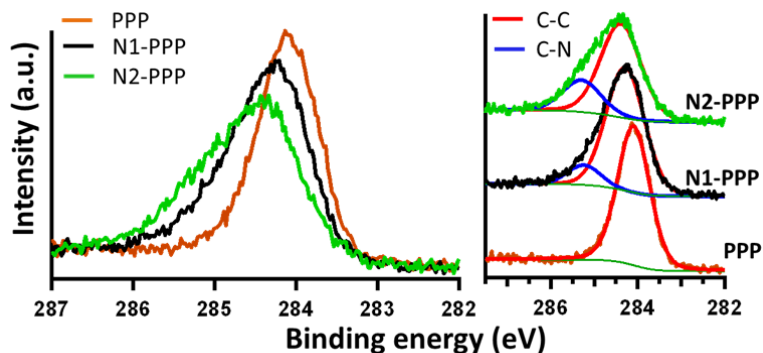

Figure S8: C 1s (hv=400 eV) XPS signals of the different polymers obtained after annealing at 180°C for 20 minutes (left). The deconvolutions (right) have been performed according to the stoichiometric ratios between carbon-linked-to-carbon (C-C) and carbon-linked-to-nitrogen (C-N) of the different precursors. In details, the ratio C-C/C-N is 7.5 and 3 for precursors 2 and 3, respectively.
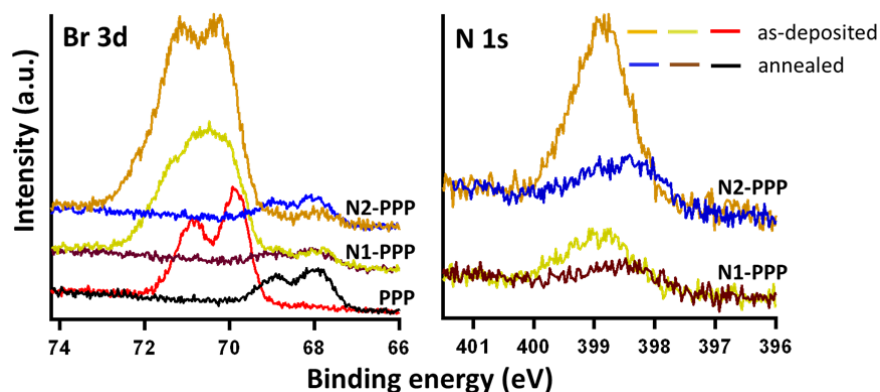

Figure S9: Br 3d and N 1s (hv=520 eV) XPS signals of the different polymers obtained after deposition and after the 20 minutes post-annealing treatment at 180°C. The as-deposited samples show that bromine is mainly linked to the organic molecule (Br $3d_{5/2} \approx 69.7$ eV), while after the heating treatment we observe a

considerable desorption and the remaining bromine is found exclusively as a chemisorbed species (Br $3d_{5/2} \approx 67.8$ eV). STM images show that adsorbed Br atoms are located in-between the poly-para-phenylene wires. In both nitrogen-doped wires, the N 1s spectra appear as a single peak centered at 398.5 eV, in good agreement with what is commonly observed for nitrogen-substituted graphene (398.2-399.3 eV),[3,4] while the C/N ratios ≈16.5 for N1-PPP and ≈11 for N2-PPP, (theoretical values are 17 and 8, respectively), further corroborate the stoichiometric insertion of the nitrogen atoms within the polymer. However, the large value of the FWHM (≈1.44 eV) suggests the presence of different subcomponents, probably due to the mismatch between the nitrogen lattice and the gold substrate resulting in N-Au bonds of varying strength.
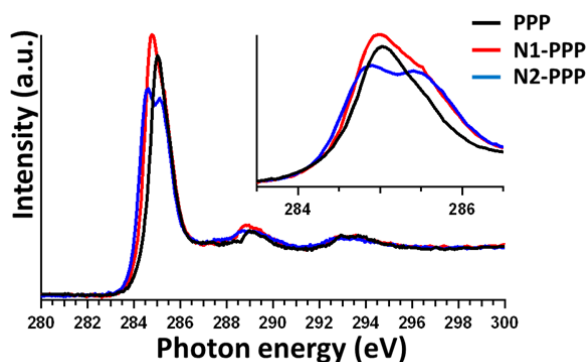

Figure S10: C K-edge NEXAFS spectra for the aligned PPP chains on Au(887). All the reported spectra have been acquired in grazing incidence geometry (θ≈30°). The inset shows a blow-up of the C 1s → π_1^* resonances.

Indirect evidences about the width of the band gaps can be gathered by probing the low-lying unoccupied states by NEXAFS spectroscopy. Figure S10 shows the experimental X-ray absorption spectra measured at the carbon threshold of the three different polymers. The largest difference is observed for the first transition at about 285 eV: a double peak structure is observed, which becomes more evident as the nitrogen content increases. Since NEXAFS spectroscopy probes resonant transitions from core levels to unoccupied states, the C 1s chemical shift between carbon-bonded and nitrogen-bonded carbon atoms is the reason of the splitting of the π_1^* band, as observed for pure pyridine.[5] Differently from photoemission spectroscopies (XPS and ARPES), NEXAFS probes resonant processes, and the relative shifts of the resonances cannot be directly compared to understand how the empty states move. In fact, nitrogen atoms affect the energy position of both the molecular and atomic states and therefore the relative NEXAFS shift between different polymers reflects the displacement of the C 1s core level with respect to the molecular empty states, see Figure S8. If the C 1s core level shifts (XPS) are compared to those probed by ARPES, it is evident that also the former are influenced by the presence of nitrogen, but the shifts are slightly smaller (The C 1s X-ray photoemission spectra have been deconvoluted in two different components, C-C and C-N, see Figure S8, according to the expected stoichiometric ratio, and the differences have been calculated between the C-C related peaks).

If we consider that the energy differences between the π_1^* transition of different polymers reflect the relative shifts of the LUMO level with respect to the C 1s core level and that a downshift is observed experimentally, we conclude that the LUMO level moves towards higher binding energy as well. Such evidences independently corroborate the STS measurements and provide a surface-averaged evaluation of the polymers electronic structure.
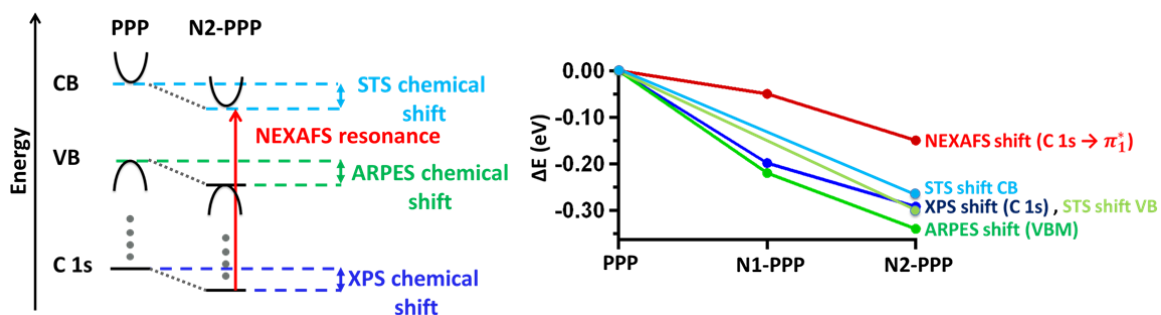
Figure S11: The left image is a diagrammatic representation of how the insertion of nitrogen affects the molecular/atomic energy levels. The techniques used to probe the displacements are listed next to each level. The right graph reports the experimentally determined shifts with respect to the PPP polymer.
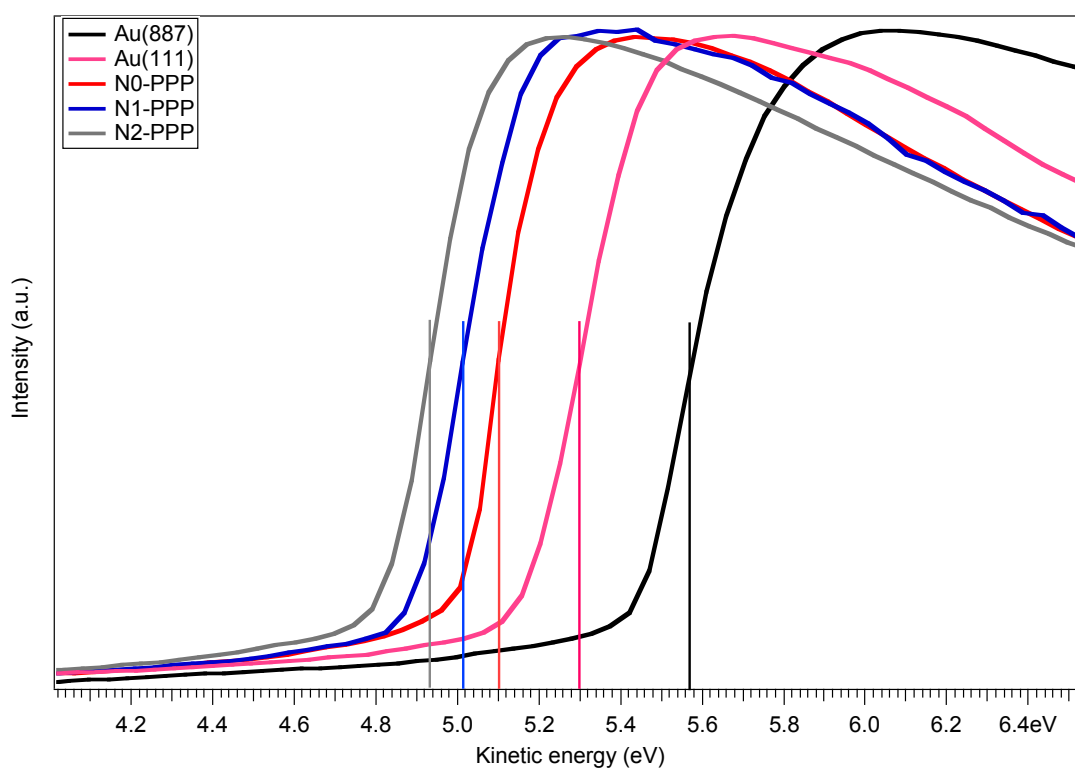

Figure S12: Secondary electron cut-off of photoemission spectra (hv=21.2 eV) revealing the work functions (WF) of clean Au(887) and Au(111), as well as of polymer-covered Au(887) surfaces. The difference between the WF of the two clean surfaces is around 0.27 eV, very similar to the difference reported between the ARPES valence band maximum of PPP on Au(887), that lies at -1.04 eV, and the onset of valence band detected by STS on PPP on Au(111), that is around -1.3 eV.
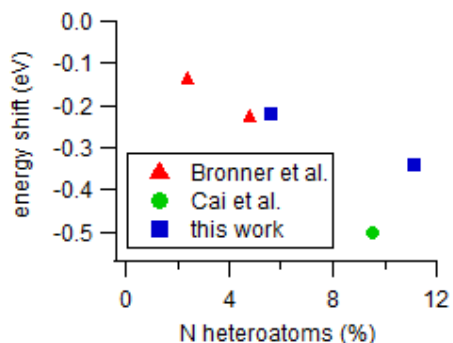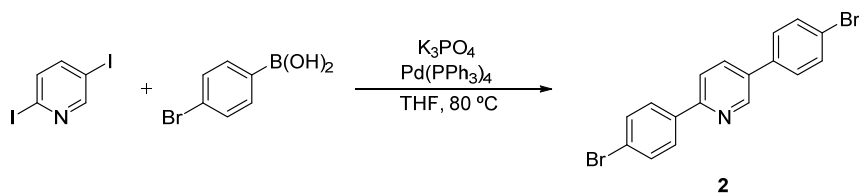
Figure S13: Valence band offset as a function of the fraction of nitrogen heteroatoms in one-dimensional extended conjugated systems. Data from this work, as well as from references [6, Bronner *et al*.] and [7, Cai *et al*.].

Experimental Section

Synthesis of 2,5-bis(4-bromophenyl)pyridine (2).

K_3PO_4 (1.03 g, 4.8 mmol) and $Pd(PPh_3)_4$ (69 mg, 0.060 mmol) were added to a stirred solution of 2,5-diiodopyridine (200 mg, 0.60 mmol) and (4-bromophenyl)boronic acid (480 mg, 2.4 mmol) in THF (15 mL). The resulting mixture was refluxed for 16 h under argon. This mixture was subsequently concentrated under reduced pressure, CH_2Cl_2 (50 mL) was added and the resulting solution was washed with H_2O (2 x 25 mL) and brine (25 mL). The organic phase was dried over Na_2SO_4, filtered and the solvent was removed under reduced pressure. The residue was purified by column chromatography (SiO_2; hexane / CH_2Cl_2, 3:2 to 1:9) to afford **2** (92 mg, 40%) as a white solid (mp 246-248 ºC). RMN analysis matches with the published data.[8]

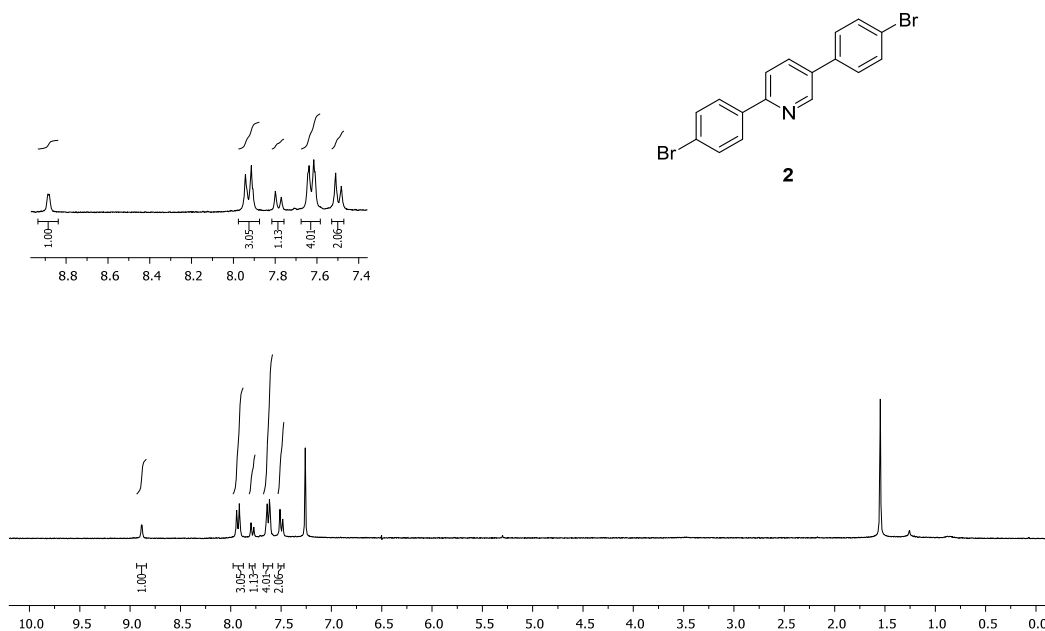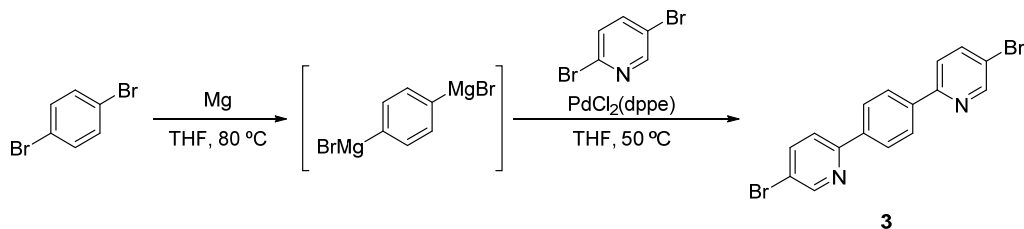^{1}H NMR spectrum is reported in figure SI14.

Figure S14: ^{1}H NMR (300 MHz, CDCl$_3$) δ 8.88 (d, J = 1.9 Hz, 1H), 7.93 (d, J = 8.5 Hz, 3H), 7.78 (d, J = 8.3 Hz, 1H), 7.63 (d, J = 6.6 Hz, 4H), 7.50 (d, J = 8.3 Hz, 2H) ppm.

Synthesis of 1,4-bis(5-bromopyridin-2-yl)benzene (3).

A published method was followed with some modifications.[9]

To a suspension of magnesium turnings (112 mg, 4.66 mmol) in dry THF (1 mL) a solution of 1,4-dibromobenzene (500 mg, 2.12 mmol) in dry THF (5 mL) was added dropwise at room temperature and then refluxed for 17 h under argon. After cooling, the resulting mixture was slowly added to a solution of 2,5-dibromopyridine (753 mg, 3.18 mmol) and PdCl$_2$(dppe) (122 mg, 0.21 mmol) in dry THF (5 mL) and the resulting mixture was heated at 50 ºC for 16 h. The mixture was then poured into water (30 mL) and extracted with CH$_2$Cl$_2$ (30 mL). The organic layer was dried over Na$_2$SO$_4$, filtered and evaporated under reduced pressure. The residue was purified by column chromatography (SiO$_2$; CH$_2$Cl$_2$) to yield **3** (41 mg, 7%) as a colorless solid (mp 258-260 ºC). ^{1}H NMR spectrum is reported in figure SI15 .
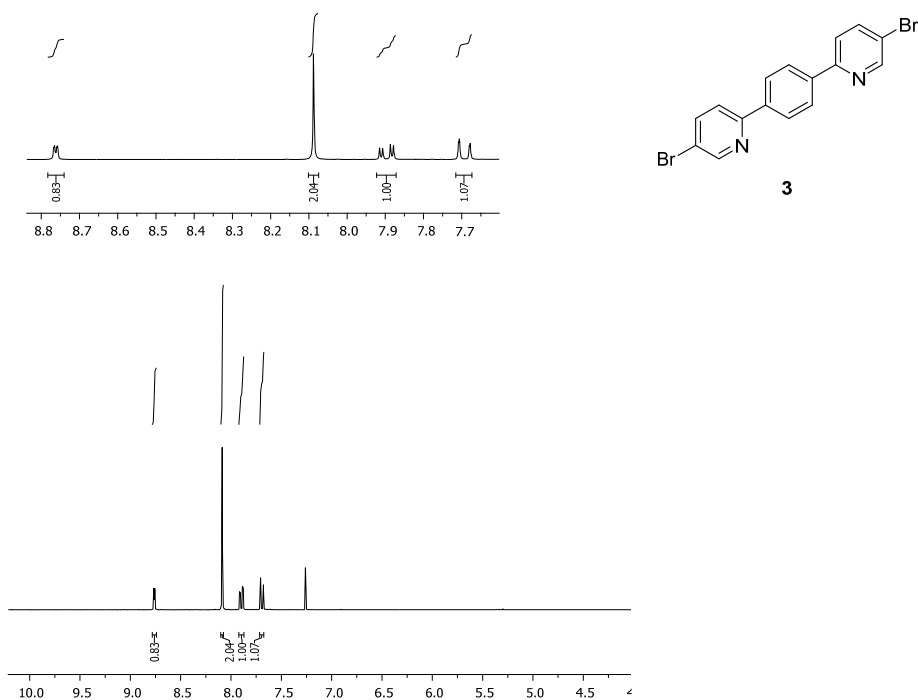
Figure S15: ^{1}H NMR (300 MHz, CDCl$_3$) δ 8.76 (dd, *J* = 2.3, 0.6 Hz, 1H), 8.09 (s, 2H), 7.90 (dd, *J* = 8.5, 2.4 Hz, 1H), 7.69 (dd, *J* = 8.5, 0.6 Hz, 1H) ppm.

Additional Computational Details.

Comparison of the adsorption geometries of the wires from DFT calculations and from NEXAFS experiments reveals that the calculated dihedral angle is lower than the experimental one, varying between 7° and 19° depending on the chain and the registry with the substrate. This is related to the well-known problem of correcting standard DFT in order to account for vdW interactions. Here, state of the art approaches still rely on empirical or semi-empirical models and significant differences between simulated and experimental geometries may easily result from an over- or underestimation of the vdW interaction. The computed electronic properties are quite stable with respect to the underestimation of the dihedral angle.

To compute the band structures of figure SI3 we used the Quantum-Espresso package.[10] To account for the vdW interaction between substrate and adsorbate we used the VDW-DF2-B86R exchange correlation functional.[11] Atomic positions were relaxed until forces were lower than 1×10^{-4} a.u. We used a shifted grid of 6x6 k-point for the Brillouin zone sampling. The slab contained 6 Au layers and a layer of hydrogen atoms to suppress the Au surface state on one side of the slab. The surface area of the slab corresponded to 6 rectangular units (8.8 Å x 10.2 Å) containing a PPP repeat unit consisting of two phenyl rings.

[1] Basagni, A.; Sedona, F.; Pignedoli, C. A.; Cattelan, M.; Nicolas, L.; Casarin, M.; Sambi, M. Molecules–Oligomers–Nanowires–Graphene Nanoribbons: A Bottom-Up Stepwise On-Surface Covalent Synthesis Preserving Long-Range Order. *J. Am. Chem. Soc.* **2015**, *137*, 1802–1808.

[2] Stöhr, J.; Outka, D. A. Determination of Molecular Orientations on Surfaces from the Angular Dependence of Near-Edge X-Ray-Absorption Fine-Structure Spectra. *Phys. Rev. B* **1987**, *36*, 7891–7905.

[3] Usachov, D.; Vilkov, O.; Grüneis, A.; Haberer, D.; Fedorov, A.; Adamchuk, V. K.; Preobrajenski, A. B.; Dudin, P.; Barinov, A.; Oehzelt, M.; Laubschat, C.; Vyalikh, D. V. Nitrogen-Doped Graphene: Efficient Growth, Structure, and Electronic Properties *Nano Lett.* **2011**, *11*, 5401–5407.

[4] Usachov, D.; Fedorov, A.; Vilkov, O.; Senkovskiy, B.; Adamchuk, V. K.; Yashina, L. V.; Volykhov, A. A.; Farjam, M.; Verbitskiy, N. I.; Grüneis, A.; Laubschat, C.; Vyalikh, D. V. The Chemistry of Imperfections in N-Graphene. *Nano Lett.* **2014**, *14*, 4982–4988.

[5] Magnuson, M.; Yang, L.; Guo, J.-H.; Såthe, C.; Agui, A.; Nordgren, J.; Luo, Y.; Ågren, H.; Johansson, N.; Salaneck, W. R.; Horsburgh, L. E.; Monkman, A. P. The Electronic Structure of Poly(Pyridine-2,5-Diyl) Investigated by Soft X-Ray Absorption and Emission Spectroscopies. *Chem. Phys.* **1998**, *237*, 295–304.

[6] Bronner, C.; Stremlau, S.; Gille, M.; Brauße, F.; Haase, A.; Hecht, S.; Tegeder, P. Aligning the Band Gap of Graphene Nanoribbons by Monomer Doping. *Angew. Chem. Int. Ed.* **2013**, *52*, 4422–4425.

[7] Cai, J.; Pignedoli, C. A.; Talirz, L.; Ruffieux, P.; Söde, H.; Liang, L.; Meunier, V.; Berger, R.; Li, R.; Feng, X.; Müllen, K.; Fasel, R. Graphene Nanoribbon Heterojunctions. *Nat. Nanotechnol.* **2014**, *9*, 896–900

[8] Kumar, A.; Rhodes, R. A.; Spychala, J.; Wilson, W. D.; Boykin, D. W.; Tidwell, R. R.; Dykstra, C. C; Hall, J. E.; Jones, S. K.; Schinazi, R. F. Synthesis of Dicationic Diarylpyridines as Nucleic-Acid Binding Agents. *Eur. J. Med. Chem.* **1995**, *30*, 99-106.

[9] Yasuda, T.; Yamamoto, T. Synthesis and Characterization of New Luminescent 1,10-Phenanthroline- and Pyridine-Containing π-Conjugated Polymers. Their Optical Response to Protic Acid, Mn+, and Solvents. *Macromolecules* **2003**, *36*, 7513-7519.

[10] Giannozzi P.; Baroni, S.; Bonini, N.; Calandra, M.; Car, R.; Cavazzoni, C.; Ceresoli, D.; Chiarotti, G. L.; Cococcioni, M.; Dabo, I.; Dal Corso, A.; de Gironcoli, S.; Fabris, S.; Fratesi, G.; Gebauer, R.; Gerstmann, U.; Gougoussis, C.; Kokalj, A.; Lazzeri, M.; Martin-Samos, L.; *et al*. QUANTUM ESPRESSO: a Modular and Open-Source Software Project for Quantum Simulations of Materials. *J. Phys.: Condens. Mat*. **2009**, *21*, 395502

[11] Lee, K.; Murray, É. D.; Kong, L.; Lundqvist, B. I.; Langreth, D. C. Higher-Accuracy van der Waals Density Functional. *Phys. Rev. B* **2010**, 82, 081101